16

Modelling and simulation of the dynamic behavior of an oil wave journal bearing

Nicoleta M. Ene, Florin Dimofte and Abdollah A. Afjeh
The University of Toledo
U.S.A.

1. Introduction

The dynamic stability of journal bearings is an important problem for rotating machinery because the dynamic properties of the bearing have a direct influence on machine stability and safety.
Because of their simplicity and large capacity, the plain journal bearings are frequently used in rotating machinery; however they can become unstable under small loads and have the tendency to generate a whirl motion with a frequency of about one half the rotational frequency of the shaft. The radius of the whirl orbit can rapidly increase so that the shaft and the sleeve can come into contact, a phenomenon that would damage the bearing. Therefore the study of the dynamic behavior of the journal bearings, especially after the instability occurs, is of theoretical and practical importance.
The bearing stability can be improved by adding grooves and holes or by reshaping the bearing surface from perfectly circular to one that incorporates lobes, offsets, tilting pads, etc. The main disadvantage of these methods is that any gain in the bearing stability may reduce the maximum load carrying capacity.

2. The Wave Bearing Concept

An alternative method to improve journal bearing stability was proposed by Dimofte (Dimofte 1995 a; Dimofte 1995 b). His concept called "wave bearing" circumscribed a continuous waved profile onto the non-rotating bearing surface. The wave amplitude is usually a fraction of the nominal bearing clearance. To exemplify the concept, a comparison between a wave bearing having circumscribed a three–wave profile and a plain journal bearing is presented in Fig. 1. In order to visualize the concept, the wave amplitude and the clearance are greatly exaggerated in Fig. 1.
The most important parameters of a wave bearing are presented in Fig. 2. In Fig. 2, a wave bearing having a three-wave profile is presented. The radial clearance C of the wave bearing is defined as the difference between the radius of the mean circle of the waves R_{med} and the radius, R, of the shaft:

$$C = R_{med} - R \tag{1}$$

The radial clearance is usually less than one thousandth of the journal radius.

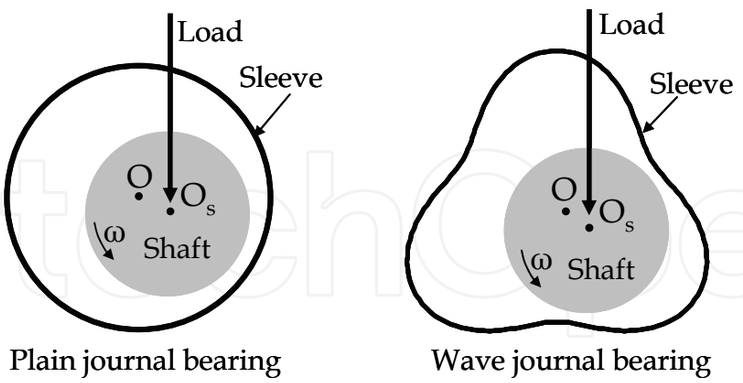

Fig. 1. Comparison between the plain journal bearing and the wave journal bearing

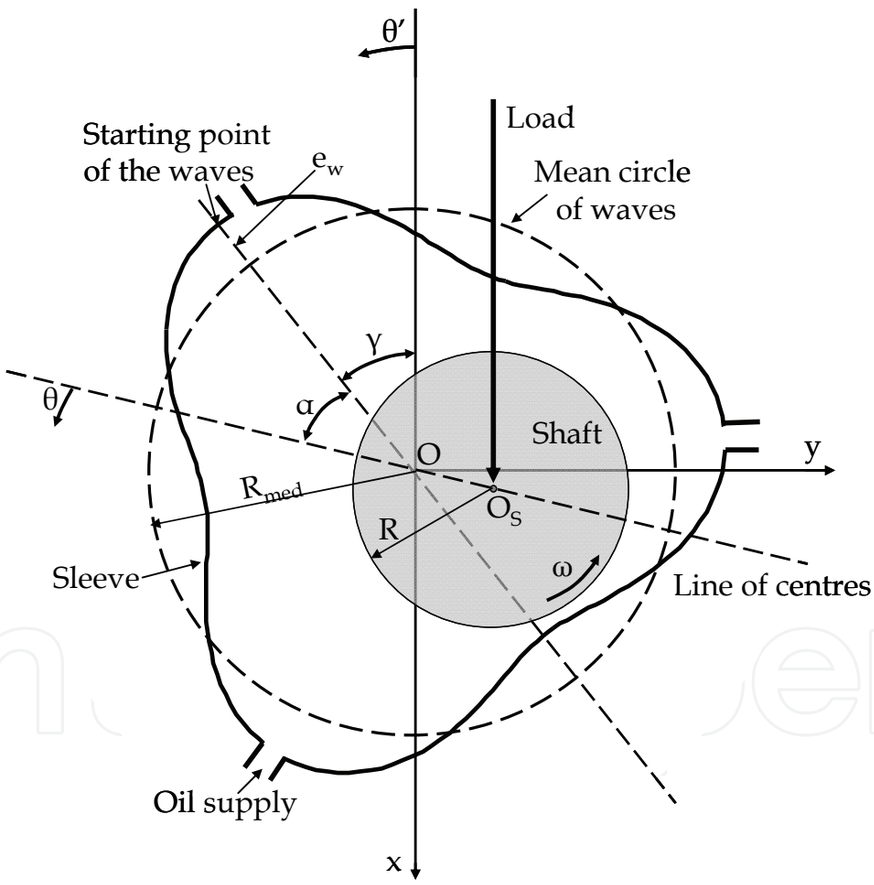

Fig. 2. The geometry of a wave journal bearing

For computational purposes, the wave amplitude is usually non-dimensionalised by dividing it by clearance:

$$\varepsilon_w = \frac{e_w}{C} \tag{2}$$

The ratio ε_w is usually called the wave amplitude ratio. The wave amplitude ratio is one of the most important geometrical characteristics of a wave bearing because the performance of the wave bearing is strongly influenced by this ratio (Ene et all., 2008). The wave amplitude ratio has values that generally range between 0.033 and 0.5.
The performance of a wave bearing also depends on the number of the waves, n_w, and on the position of the waves relative to the direction of the load, W. Theoretical and experimental studies indicate that the best performance is obtained by a three-wave bearing having one of the points with maximum wave amplitude on the direction of the load (Dimofte, 1995 a, Dimofte, 1995 c).
The load capacity of a wave bearing is due to the rotation of the shaft and to the variation of film thickness along the circumference. With some geometrical considerations, it can be shown that in a system of coordinates rotating with the line of centres the fluid film thickness h is given by:

$$h = C + e\cos\theta + e_w \cos\left[n_w(\theta + \alpha)\right] \tag{3}$$

where θ is the angular coordinate starting from the line of centres and α is the angle between the starting point of the waves and the line of centres. The film thickness can be also expressed in a system of reference Oxy fixed with respect to the sleeve:

$$h = C + e_w \cos\left[n_w(\theta' - \gamma)\right] + x_s \cos\theta' + y_s \sin\theta' \tag{4}$$

where θ' is the angular coordinate starting from the negative Ox axis, γ is the angle between the starting point of the waves and the vertical axis and (x_s,y_s) are the coordinates of the rotor centre.
Because the shape of a wave bearing is very close to the shape of a plain journal bearing, the loss of load capacity of the wave bearing compared to the plain journal bearing is minimal (Dimofte, 1995 a).
The wave bearing concept also includes a number of supply pockets equal to the number of the waves (see Fig. 2). They are situated near the points where the waves have maximum values.

3. Methods for Simulating the Dynamic Behavior of a Wave Journal Bearing

Since the early paper of Newkirk and Taylor (Newkirk & Taylor, 1925), a considerable number of papers have been devoted to the study of the dynamic stability of the journal bearings. Two types of approaches can be identified:
- critical mass approaches based on small-perturbation theories;
- transient approaches based on linear or non-linear theories.

The critical mass approach has been very popular because of its simplicity and limited computational requirements. The main disadvantage of this method is that no bearing information can be obtained after the appearance of an unstable whirl. The bearing dynamic behavior for unstable conditions can be predicted only by using transient methods. The main disadvantage of the transient methods is that they require a large amount of computational time.

Calculation of the critical mass implies in the first stage the computation of the dynamic coefficients. Two methods can be used to compute the dynamic coefficients:
- numerical differentiation of the pressure distributions with respect to small perturbations of displacements and velocities of the journal centre;
- perturbation methods.

The numerical differentiation method requires correct identification of the values of the small perturbations so that they are small enough to remain within the limits of the linear theory, but large enough to produce significant perturbations with respect to numerical errors and approximations. (Frêne et al., 1997). The numerical differentiation method can be used to calculate the dynamic coefficients for different types of journal bearings: circular journal bearings (Orcutt & Arvas, 1967; Parkins, 1979), tilting pad journal bearings (White & Chan, 1992), etc.

The problem of correct selection of the small perturbation values can be eliminated by using a perturbation method. The perturbation method was first introduced by Lund (Lund & Thomsen, 1978; Lund 1984; Kilt & Lund, 1986). It consists of solving five partial differential equations, one corresponding to the steady-state pressure distribution and the other four to the pressure gradients. The dynamic coefficients are then calculated by integrating the pressure gradients distributions. Lund's approach has been used by many authors to compute the dynamic characteristics of different types of bearings. For example, Lund's method was used by Kostrzewsky et al. (Kostrzewsky et al., 1998) to compute the dynamic characteristics of highly preloaded three-lobe journal bearings. In order to reduce the computation time, the authors assumed a polynomial form for the axial pressure distribution. Kakoty and Majumdar (Kakoty & Majumdar, 1999; Kakoty & Majumdar, 2000) studied the effect of fluid inertia on the stability of oil film journal bearings also using a linear perturbation analysis. Rao and Sawicki adapted Lund's infinitesimal procedure so that the film content at cavitation rupture and deformation boundaries is taken into consideration for both a steady-state pressure distribution and dynamic pressure gradients. Rao and Sawicki used this method to investigate the stability characteristics of journal bearings (Rao & Sawicki, 2002) and herringbone grooved journal bearings (Rao & Sawicki, 2004).

Many papers have investigated the dynamic stability of journal bearings using a transient approach. One of the first transient analyses of a journal bearing was performed by Kirk and Gunter (Kirk & Gunter, 1976a; Kirk & Gunter, 1976b). Because of the computation limitations, they determined the fluid film forces by using a short bearing approximation.

Monmousseau and Fillon (Monmousseau & Fillon, 1999) used a non-linear transient approach to analyze the dynamic behavior of a tilting–pad journal bearing submitted to a synchronous and a non-synchronous load. The authors showed that the amplitude of the shaft orbit is maximum when the loading frequency is near the critical frequency.

San Andres (San Andres, 1997) compared the transient responses of a rigid rotor supported on externally pressurized, turbulent fluid film bearings obtained using two different models: an approximate model based on constant rotordynamic coefficients and a full nonlinear model. He concluded that the approximate model provided accurate results only for small amplitude loadings and for operating conditions far enough from the stability margin of the rotor bearing system.

Tieu and Qiu (Tieu & Qiu, 1995) presented a comparison between the journal centre trajectories of a journal bearing computed using both non-linear and linear theory. Both

methods provided the same critical speed. However, under large dynamic excitations, the trajectories obtained with the two methods were significantly different.
Tichy and Bou-Said (Tichy & Bou-Said, 1991) and Hashimoto and Wada (Hashimoto & Wada, 1990) used transient methods to emphasize the effects of turbulence on the dynamic response of rotors supported in journal bearings.
Vijayaraghavan and Brewe (Vijayaraghavan & Brewe, 1992) predicted the trajectories of a hydrodynamic journal bearing when a unidirectional external periodic load is applied. The authors reported that under periodic loads, the journal centre almost always attains a stable limit cycle. When the loading frequency is half of the journal frequency, the fluid film forces become very large and the journal centre whirls at large eccentricities.
In this paper both a critical mass approach and a transient method will be used to predict the dynamic behavior of a three-wave bearing in the absence of any external load.

4. Critical Mass Approach

4.1 Governing equations

The small perturbation theory assumes that the shaft motion is stable and is limited to small perturbations around the static equilibrium. Suppose that in the fixed system of reference Oxy (see Fig. 2), the journal centre position is characterized in the steady-state regime by coordinates (x_{s0}, y_{s0}). The corresponding film thickness will be denoted by h_0. Because the shaft motion is limited to small perturbations, the shaft position in the dynamic regime (x_s, y_s) can be described by small amplitudes from the static equilibrium:

$$\begin{aligned} x_s &= x_{s0} + \Delta x \\ y_s &= y_{s0} + \Delta y \end{aligned} \tag{5}$$

By combining Eqs. 4 and 5, a relation between the film thicknesses corresponding to the steady state (h_0) and dynamic regimes (h) is obtained:

$$h = h_0 + \Delta x \cos\theta' + \Delta y \sin\theta' \tag{6}$$

Similarly, the dynamic pressure p can be expressed as a first order Taylor expansion around the steady-state pressure p_0:

$$p = p_0 + p_x \Delta x + p_y \Delta y + p_{\dot{x}} \Delta \dot{x} + p_{\dot{y}} \Delta \dot{y} \tag{7}$$

The pressure distribution in the wave journal bearing is described by the Reynolds equation:

$$\frac{1}{R^2}\frac{\partial}{\partial\theta}\left(\frac{h^3}{k_\theta \mu}\frac{\partial p}{\partial\theta}\right) + \frac{\partial}{\partial z}\left(\frac{h^3}{k_z \mu}\frac{\partial p}{\partial z}\right) = \frac{\partial h}{\partial t} + \frac{\omega}{2}\frac{\partial h}{\partial\theta} \tag{8}$$

where p is the dynamic pressure, h - the fluid film thickness, R - the bearing radius, ω – the rotational speed, μ – lubricant viscosity, t-time, θ –angular coordinate, z – axial coordinate, and k_θ, k_z are correction coefficients for turbulent flow. The Reynolds equation can be

obtained from the general Navier-Stocks equations by considering that the dimension upon the film thickness is very small compared to the two other directions.
By introducing the pressure expansion (Eq. 7) and the film thickness equation (Eq. 6) into the Reynolds equation (Eq. 8), developing a series and retaining only first order terms, five partial differential equations are obtained:

$$\frac{1}{R^2}\frac{\partial}{\partial\theta'}\left(\frac{h^3}{k_\theta\mu}\frac{\partial p_0}{\partial\theta'}\right)+\frac{\partial}{\partial z}\left(\frac{h^3}{k_z\mu}\frac{\partial p_0}{\partial z}\right)=\frac{\omega}{2}\frac{\partial h}{\partial\theta'} \tag{9a}$$

$$\frac{1}{R^2}\frac{\partial}{\partial\theta'}\left(\frac{h^3}{k_\theta\mu}\frac{\partial p_x}{\partial\theta'}\right)+\frac{\partial}{\partial z}\left(\frac{h^3}{k_z\mu}\frac{\partial p_x}{\partial z}\right)=-\frac{\omega}{2}\left(\sin\theta'+3\frac{\cos\theta'}{h}\frac{\partial h}{\partial\theta'}\right)-\frac{h^3}{4\mu R^2}\frac{\partial p_0}{\partial\theta'}\frac{\partial}{\partial\theta'}\left(\frac{\cos\theta'}{h}\right) \tag{9b}$$

$$\frac{1}{R^2}\frac{\partial}{\partial\theta'}\left(\frac{h^3}{k_\theta\mu}\frac{\partial p_y}{\partial\theta'}\right)+\frac{\partial}{\partial z}\left(\frac{h^3}{k_z\mu}\frac{\partial p_y}{\partial z}\right)=\frac{\omega}{2}\left(\cos\theta'-3\frac{\sin\theta'}{h}\frac{\partial h}{\partial\theta'}\right)-\frac{h^3}{4\mu R^2}\frac{\partial p_0}{\partial\theta'}\frac{\partial}{\partial\theta'}\left(\frac{\sin\theta'}{h}\right) \tag{9c}$$

$$\frac{1}{R^2}\frac{\partial}{\partial\theta'}\left(\frac{h^3}{k_\theta\mu}\frac{\partial p_{\dot{x}}}{\partial\theta'}\right)+\frac{\partial}{\partial z}\left(\frac{h^3}{k_z\mu}\frac{\partial p_{\dot{x}}}{\partial z}\right)=\cos\theta' \tag{9d}$$

$$\frac{1}{R^2}\frac{\partial}{\partial\theta'}\left(\frac{h^3}{k_\theta\mu}\frac{\partial p_{\dot{y}}}{\partial\theta'}\right)+\frac{\partial}{\partial z}\left(\frac{h^3}{k_z\mu}\frac{\partial p_{\dot{y}}}{\partial z}\right)=\sin\theta' \tag{9e}$$

For the above equations, the Reynolds boundary conditions at the film rupture zones are:

$$p_0=\frac{\partial p_0}{\partial\theta'}=\frac{\partial p_0}{\partial z}=0 \qquad p_x=p_y=p_{\dot{x}}=p_{\dot{y}} \tag{10}$$

The boundary conditions at the axial ends of the bearing are:

$$p_0=p_{ext} \qquad p_x=p_y=p_{\dot{x}}=p_{\dot{y}} \tag{11}$$

where p_{ext} is the external pressure. Similarly, the boundary conditions corresponding to the supply pockets are:

$$p_0=p_s \qquad p_x=p_y=p_{\dot{x}}=p_{\dot{y}} \tag{12}$$

where p_s is the supply pressure.
It can be seen that Eq. 9a corresponds to the steady-state regime. If the external force is vertical, then the equilibrium equations are:

$$\begin{bmatrix} -W \\ 0 \end{bmatrix} = R \int_{-\frac{L}{2}}^{\frac{L}{2}} \int_{0}^{2\pi} p_0 \begin{bmatrix} \cos\theta' \\ \sin\theta' \end{bmatrix} d\theta' dz \tag{13}$$

The solutions of Eqs. 9b-d allow one to determine the stiffness and damping coefficients of the bearing:

$$\begin{bmatrix} K_{xx} & K_{xy} \\ K_{yx} & K_{yy} \end{bmatrix} = R \int_{-\frac{L}{2}}^{\frac{L}{2}} \int_{0}^{2\pi} \begin{bmatrix} p_x \cos\theta' & p_y \cos\theta' \\ p_x \sin\theta' & p_y \sin\theta' \end{bmatrix} d\theta' dz \tag{14}$$

$$\begin{bmatrix} B_{xx} & B_{xy} \\ B_{yx} & B_{yy} \end{bmatrix} = R \int_{-\frac{L}{2}}^{\frac{L}{2}} \int_{0}^{2\pi} \begin{bmatrix} p_{\dot{x}} \cos\theta' & p_{\dot{y}} \cos\theta' \\ p_{\dot{x}} \sin\theta' & p_{\dot{y}} \sin\theta' \end{bmatrix} d\theta' dz \tag{15}$$

The upper limit of the stability is given by the critical mass:

$$m_{cr} = \frac{K_s}{\gamma_s^2} \tag{16}$$

where K_s is the effective bearing stiffness:

$$K_s = \frac{B_{xx}K_{yy} + B_{yy}K_{xx} - B_{xy}K_{yx} - B_{yx}K_{xy}}{B_{xx} + B_{yy}} \tag{17}$$

and γ_s is the instability whirl frequency:

$$\gamma_s = \sqrt{\frac{(K_{xx} - K_s)(K_{yy} - K_s) - K_{xy}K_{yx}}{B_{xx}B_{yy} - B_{xy}B_{yx}}} \tag{18}$$

The critical mass delimitates two possible equilibrium cases:

1. The rotor mass is smaller than the critical mass ($m < m_{cr}$). The rotor centre returns to its static equilibrium position. Particularly, in absence of any external load, the rotor centre rotates with a small radius around the bearing centre. The radius depends on the shaft run-out. In this case, the operating point is stable.
2. The rotor mass is greater than the critical mass ($m > m_{cr}$). The rotor centre leaves its static position and the equilibrium point is unstable. In this case, the method does not allow one to predict the motion of the journal centre.

4.2 Turbulence model

Constantinescu's model of turbulence (Constantinescu et all., 1985; Frêne & Constantinescu, 1975), which is based on Prandtl mixing length hypothesis, was chosen to model the turbulence effects. According to this model, the first signs of turbulence appear when the mean Reynolds number, Re_m, is equal to the critical Reynolds number, Re_{cr}:

$$Re_m = Re_{cr} \tag{19}$$

where:

$$Re_m = \frac{2\rho q}{\mu} \tag{20}$$

$$Re_{cr} = \min\left(41.2\sqrt{\frac{R}{h}}, 2000\right) \tag{21}$$

and q is the total flow. The flow becomes turbulent when:

$$Re_m = 2\,Re_{cr} \tag{22}$$

With these assumptions, the coefficients for turbulent flow are given by:

$$\begin{aligned} k_\theta &= 12 + 0.0136\,Re_{eff}^{0.9} \\ k_z &= 12 + 0.0044\,Re_{eff}^{0.9} \end{aligned} \tag{23}$$

where:

$$Re_{eff} = \begin{cases} 0 & Re_m < Re_{cr} \\ \left(\frac{Re_m}{Re_{cr}} - 1\right)\frac{\rho R\omega h}{\mu} & Re_{cr} \le Re_m \le 2Re_{cr} \\ \frac{\rho R\omega h}{\mu} & Re_m > 2Re_{cr} \end{cases} \tag{24}$$

4.3 Model for thermal effects

Due to computational time considerations, a constant mean temperature is assumed throughout the film. The value of the mean temperature is obtained from a global energy balance on the bearing. An adiabatic model is considered for the energy balance. According to the adiabatic model, all the energy dissipated in the fluid film is convected away by the lubricant. Consequently, the heat generated by friction causes only an increase of the lubricant temperature. Therefore, the increase of the lubricant temperature (the difference

between the temperature of the lubricant entering the film and the constant mean temperature of the film) is given by:

$$\Delta T = \frac{F_f R\omega}{\rho c_v q_{lat}} \tag{25}$$

where c_v is the lubricant specific heat, q_{lat} is the rate of lateral flow and F_f is the friction force. The friction force can be obtained by integrating the friction stresses on the bearing surfaces:

$$(\tau)_{0,h} = \frac{\mu V}{h}\left(1 + 0.0012\,\mathrm{Re}_{eff}^{0.94}\right) \pm \frac{h}{2R}\frac{\partial p}{\partial \theta} \tag{26}$$

4.4 Numerical approach

The first problem that must be solved before evaluating the critical mass is to determine the equilibrium position. At the equilibrium, in absence of any external force, the fluid film force must be vertical and equal to the bearing weight. The fluid film force can be calculated by integrating the steady-state pressure distribution (Eq. 13) where the steady-state pressure distribution is described by the steady-state Reynolds equation (Eq. 9a). In the present paper the steady-state Reynolds equation is successively solved for different positions of the shaft until the fluid film force is vertical and equal to the shaft weight. A bisection algorithm was developed for this purpose.

For every position of the shaft, the turbulence correction coefficients are determined by successive iterations. Thus, for each journal centre position, at the first iteration the pressure distribution is determined by assuming that the flow is laminar (i.e., the effective Reynolds number is zero and the correction coefficients are 12). From the computed pressure distribution, new values of the correction coefficients at every grid point are determined. Also, the new mean film temperature (Eqs. 25-26) and the new lubricant properties are determined. Then the steady-state Reynolds equation (Eq. 9a) is integrated again for the new values of the correction coefficients and the new mean film temperature. The iterative process is repeated until the relative errors for the correction coefficients are smaller than a prescribed value (10^{-5}).

The steady-state Reynolds equation (Eq. 9a) is discretized with a finite difference scheme. The resultant system of equations is solved with a successive over-relaxation method (the Gauss–Seidel method).

Having the equilibrium position of the shaft and the correction coefficients corresponding to this position, the pressure gradients can now be determined by integrating the differential equations corresponding to the pressure gradients (Eqs. 9b-9e) with a finite difference scheme. The dynamic coefficients are then calculated by integrating the pressure gradients over the entire film (Eqs. 14-15) and next the critical mass is obtained with the equations Eqs. 16-18.

5. Model for simulating the bearing dynamic behavior with a transient method

5.1 Governing equations

Without any external force, the equations of motion along and perpendicular to the line of centres are:

$$\begin{aligned} m\left[\frac{d^2e}{dt^2}-e\left(\frac{d\phi}{dt}\right)^2\right] &= F_r + mg\cos\phi + m\omega^2\rho\cos(\omega t-\phi) \\ m\left(e\frac{d^2\phi}{dt^2}+2\frac{d\phi}{dt}\frac{de}{dt}\right) &= F_\phi - mg\sin\phi + m\omega^2\rho\sin(\omega t-\phi) \end{aligned} \tag{27}$$

where F_r and F_ϕ are the radial and tangential components of the fluid force, ρ - the shaft run-out, 2m- the rotor mass, and ω - the rotational velocity. The components of the fluid film force can be determined by integrating the pressure distribution:

$$\begin{aligned} F_r &= R\int_{-L/2}^{L/2}\int_0^{2\pi} p\cos\theta\, d\theta dz \\ F_\phi &= R\int_{-L/2}^{L/2}\int_0^{2\pi} p\sin\theta\, d\theta dz \end{aligned} \tag{28}$$

The pressure distribution in this case is obtained by solving the Reynolds equation written in the following form:

$$\frac{1}{R^2}\frac{\partial}{\partial\theta}\left(\frac{1}{k_\theta}\frac{h^3}{\mu}\frac{\partial p}{\partial\theta}\right)+\frac{\partial}{\partial z}\left(\frac{1}{k_z}\frac{h^3}{\mu}\frac{\partial p}{\partial z}\right)=\mu\left(\dot{e}\cos\theta+e\dot{\phi}\sin\theta+\frac{\omega}{2}\frac{\partial h}{\partial\theta}\right) \tag{29}$$

The above form of the Reynolds equation was obtained by introducing the expression for the wave bearing film thickness (Eq. 3) into Eq. 8. For Eq. 29 the Reynolds boundary conditions at the film rupture zones are:

$$p=\frac{\partial p}{\partial\theta}=\frac{\partial p}{\partial z}=0 \tag{30}$$

Constantinescu's model of turbulence is also used for this approach to model the turbulent flow.

5.2 Numerical approach

The trajectory of the journal centre is obtained by integrating in time the equations of motion (Eqs. 27). At each time step, a pressure distribution corresponding to the motion parameters ($e,\ \phi, \dot{e}, \dot{\phi}$) and correction coefficients for turbulent flow (k_θ and k_z) from the previous moment of time is first obtained. The pressure distribution is found by integrating the

Reynolds equation (Eq. 29) using a central difference scheme combined with a Gauss-Seidel method.
Then a new set of correction coefficients (Eqs. 23) corresponding to the new pressure distribution is calculated. Next an energy balance is performed and a new mean film temperature is obtained, Eq. (25). The lubricant properties (viscosity, density and specific heat) are then updated for the new mean film temperature. Afterwards, the Reynolds equation is integrated again for the new values of the correction coefficients and lubricant viscosity. The iterative process is repeated until the relative errors for the correction coefficients and for mean temperature are smaller than prescribed values. Furthermore, the fluid film forces are calculated by integrating the final pressure distribution over the entire film (Eqs. 28). All the parameters of the equations of motion (Eqs. 27) are now known so they can be integrated to determine the new position of the journal centre. A fourth order Runge–Kutta algorithm is used to integrate the motion equations. The algorithm is repeated until the orbit of the journal centre is completed.

6. Numerical simulations

Both the critical mass and the transient approaches are used to study the dynamic behavior of a three-wave bearing having a length of 27.5 mm, a radius of the mean circle of the waves of 15 mm, and a clearance of 35 microns. The rotor mass corresponding to one bearing is 0.825 kg. Synthetic turbine oil Mil-L-23699 was used as a lubricant. The numerical predictions are compared to experimental data (Dimofte et al., 2004).
In real machinery, the rotor always has a small unbalance. This unbalance can be modeled as a small run-out. For this reason, two types of transient simulations were performed: the "ideal case" with zero run-out and "the real case" with a small run-out of 2 microns. For the critical mass approach, the shaft unbalance can not be taken into consideration.
Different wave amplitude ratios, oil supply pressures and inlet temperatures were considered for simulations. The experimental studies showed that for a wave amplitude ratio of 0.305 the wave bearing is stable even at speeds of 60000 rpm and supply pressures of 0.152 MPa. For example, the FFT analysis and the wave shape of the signal from one of the proximity probes corresponding to a rotational speed of 60000 rpm are presented in Fig. 3. FFT analysis shows the presence of an amplitude peak only at the synchronous frequency. In addition, the regular shape of the proximity probe signals indicates also a harmonic motion. The same conclusion can be drawn from the numerical simulations. The variation of the critical mass with the rotational speed, as it was predicted by the small perturbation theory, is shown in Fig. 4. It can be seen that the critical mass is greater than the bearing mass for speeds up to 60000 rpm. Consequently, the bearing is stable for speeds up to 60000 rpm. The trajectory of the shaft centre is predicted with the transient approach. For example, the trajectory of the shaft centre for a rotational speed of 60000 rpm and a zero run-out is presented in Fig. 5. It can be seen from Fig. 5 that the journal centre approaches very rapidly to the bearing centre and orbits around it with a very small radius. When a run-out is considered, the journal centre rotates with one frequency around the bearing centre on a closed orbit having the radius approximately equal to the run-out. For example, the trajectory of the journal centre for a rotational speed of 60000 rpm and a run-out of 2 microns is shown in Fig. 6. The shaft centre motion in horizontal direction (Fig. 7) indicates a

harmonic motion. The FFT analysis of the shaft centre motion in horizontal direction (Fig.8) shows that the frequency of the journal centre motion is equal to the rotor speed.

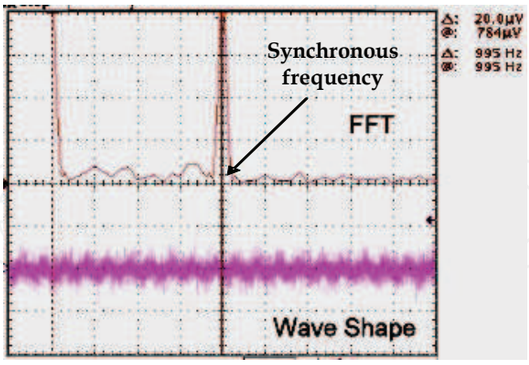

Fig. 3. FFT analysis and wave shape of the experimental signal for $\varepsilon_w = 0.305$, n=60000 rpm, p_s=0.152 MPa

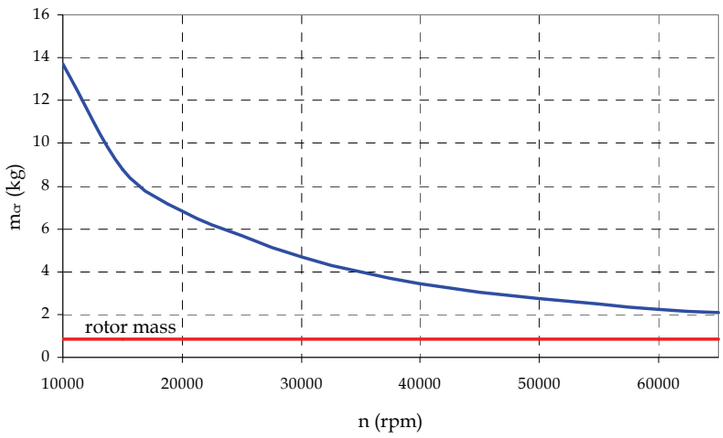

Fig. 4. Critical mass as function of running speed for $\varepsilon_w = 0.305$ and p_s=0.152 MPa

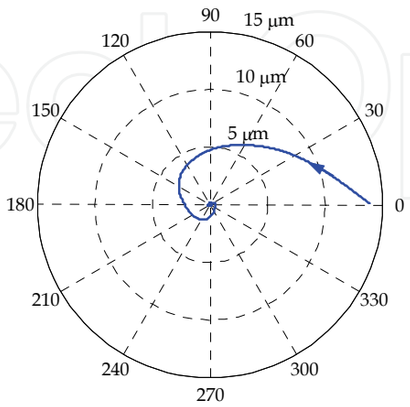

Fig. 5. Trajectory of the journal centre for $\varepsilon_w = 0.305$, n=60000 rpm, p_s=0.152 MPa , and zero run-out

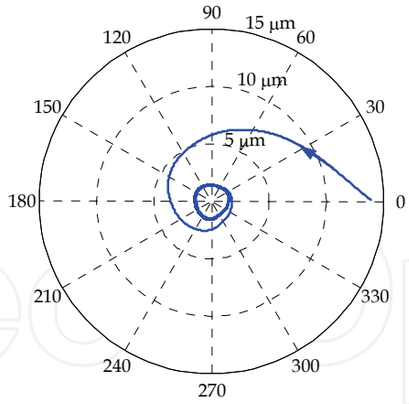

Fig. 6. Trajectory of the journal centre for $\varepsilon_w = 0.305$, n=60000 rpm, p_s=0.152 MPa , and 2 microns run-out

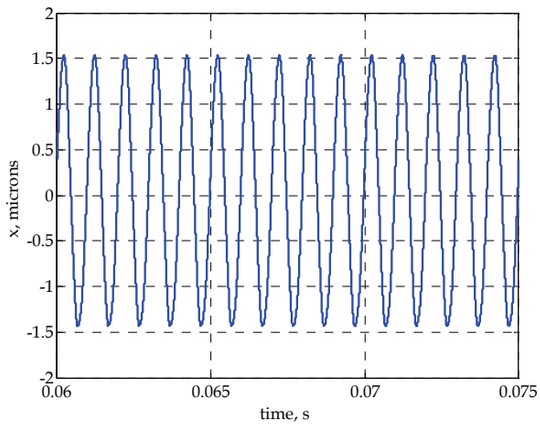

Fig. 7. The position of the shaft centre in the horizontal direction for $\varepsilon_w = 0.305$, n=60000 rpm, p_s=0.152 MPa , and 2 microns run-out

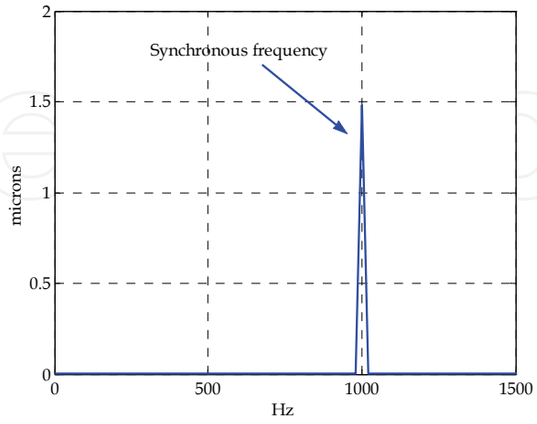

Fig. 8. FFT analysis of the motion in the horizontal direction for $\varepsilon_w = 0.305$, n=60000 rpm, p_s=0.152 MPa , and 2 microns run-out

For wave amplitude ratios smaller than 0.305, the experiments and the numerical simulations show that the rotor centre of the analyzed wave bearing can experience an unstable motion at rotational speeds that depend on the wave amplitude ratio and oil supply pressure. For example, the variation of the critical mass with the rotational speed for a wave amplitude ratio of 0.075, a supply pressure of 0.276 MPa at an oil temperature inlet of 126° C is presented in Fig. 9. It can be seen that the critical mass is greater than the mass of the shaft related to one bearing for speeds smaller than 39000 rpm. The critical mass is very close to the rotor mass around 39000 rpm and then it becomes smaller than the rotor mass. Consequently, it may be concluded that the fluid film of the wave bearing is unstable for rotational speeds greater than 39000 rpm.

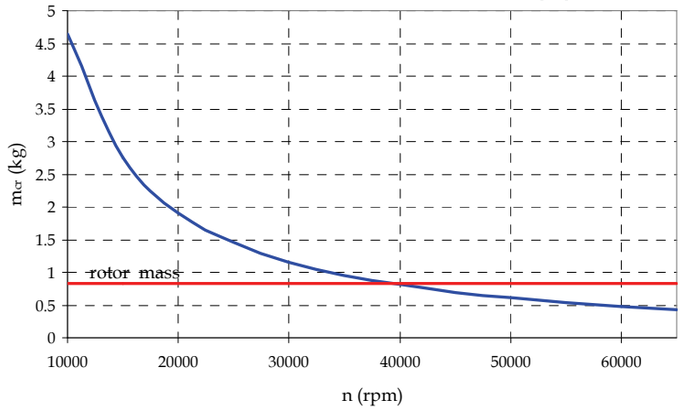

Fig. 9. Critical mass as function of running speed for $\varepsilon_w = 0.075$ and p_s=0.276 MPa

The transient analysis allows for the examination of the post whirl orbit details. The stable trajectories of the journal centre rotating at 36000 rpm with zero and 2 microns run-out are presented in Figs. 10 and 11. The FFT analyses of the numerical predicted motion (Fig. 12) and of the experimental signals from the proximity probes (Fig. 13) indicate the presence of only the synchronous frequency. The wave shapes of the motion in the horizontal direction obtained experimentally (Fig. 13) and from numerical simulations (Fig. 14) also suggest a harmonic motion.

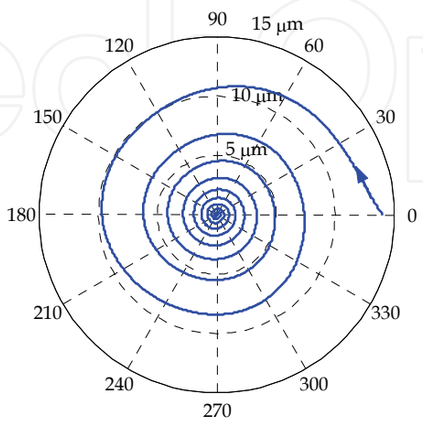

Fig. 10. Trajectory of the journal centre for $\varepsilon_w = 0.075$, n=36000 rpm, p_s=0.276 MPa , and zero run-out

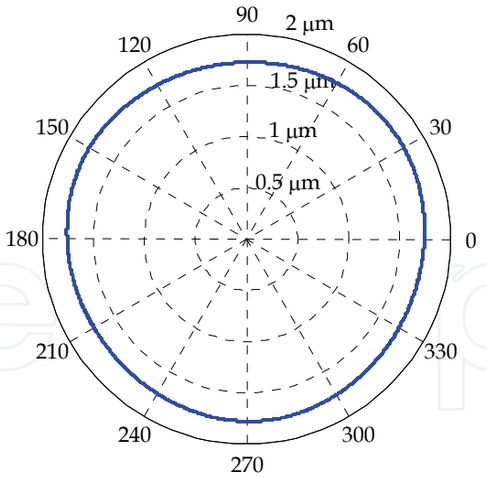

Fig. 11. Trajectory of the journal centre for $\varepsilon_w = 0.075$, n=36000 rpm, p_s=0.276 MPa , and 2 microns run-out

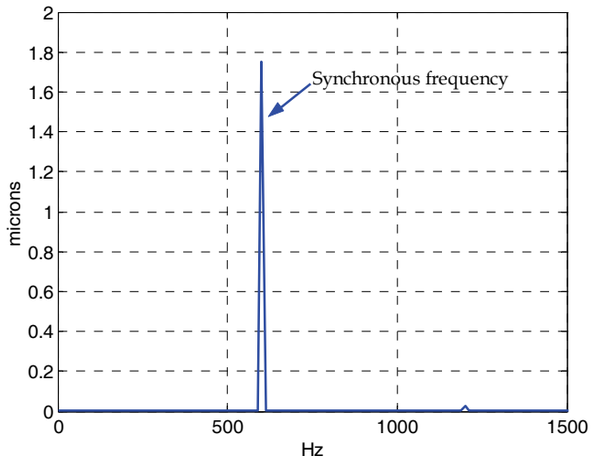

Fig. 12. FFT analysis of the motion in the horizontal direction for $\varepsilon_w = 0.075$, n=36000 rpm, ps=0.276 MPa , and 2 microns run-out

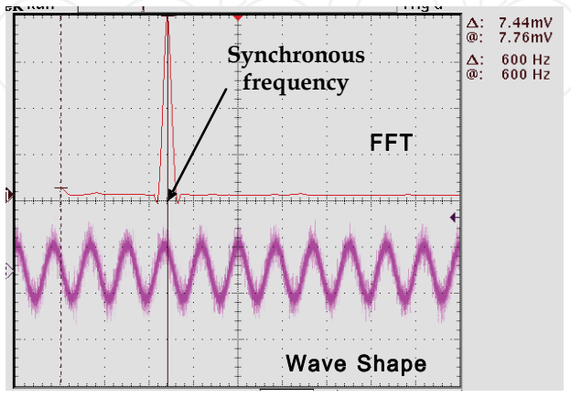

Fig. 13. FFT analysis and wave shape of the experimental signal for $\varepsilon_w = 0.075$, n=36000 rpm, p_s=0.276 MPa

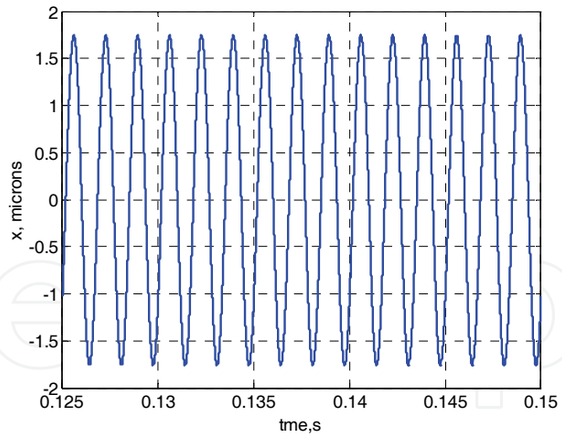

Fig. 14. The position of the shaft centre in the horizontal direction for $\varepsilon_w = 0.075$, n=36000 rpm, p_s=0.276 MPa , and 2 microns run-out

If the speed is increased to the stability threshold (39000 rpm, in this case) an incipient sub-synchronous motion can be detected. The FFT analysis and the wave shape of the signal from the proximity probes are presented in Fig. 15. In this case, both the synchronous and sub-synchronous frequencies can be identified. However, the synchronous frequency is still dominant. The simulated journal centre motion for zero unbalance is presented in Fig. 16. In this case the journal centre rotates on a closed orbit. The FFT analysis of the motion predicts only the sub-synchronous frequency (Fig. 17). The presence of the synchronous frequency can be predicted by the numerical simulations only if the rotor unbalance is taken into consideration. When the run-out is introduced in simulations, the journal centre rotates on a limit cycle with two frequencies (Fig. 18). The motion of the journal centre in the horizontal direction (Fig. 19) and the FFT analysis of the motion (Fig. 20) indicate the existence of both synchronous and sub-synchronous frequencies. They are very similar to those predicted by experiments (Fig. 15).

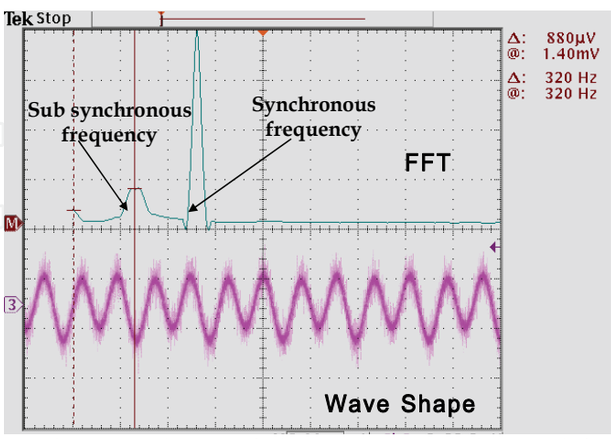

Fig. 15. FFT analysis and wave shape of the experimental signal for $\varepsilon_w = 0.075$, n=39000 rpm, ps=0.276 MPa

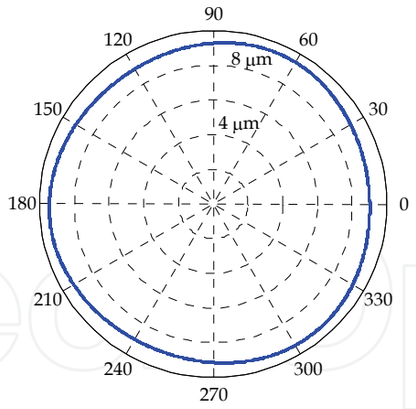

Fig. 16. Trajectory of the journal centre for $\varepsilon_w = 0.075$, n=39000 rpm, p_s=0.276 MPa , and zero run-out

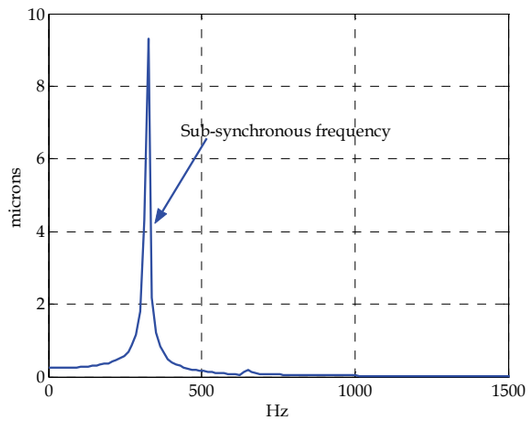

Fig. 17. FFT analysis of the motion in the horizontal direction for $\varepsilon_w = 0.075$, n=39000 rpm, p_s=0.276 MPa , and zero run-out

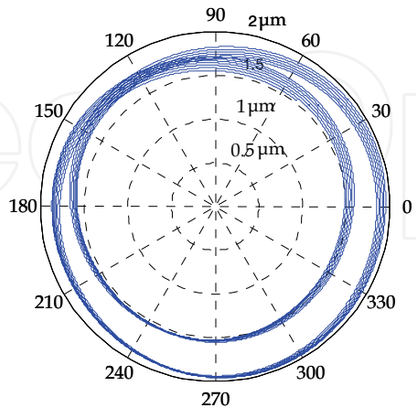

Fig. 18. Trajectory of the journal centre for $\varepsilon_w = 0.075$, n=39000 rpm, p_s=0.276 MPa , and 2 microns run-out

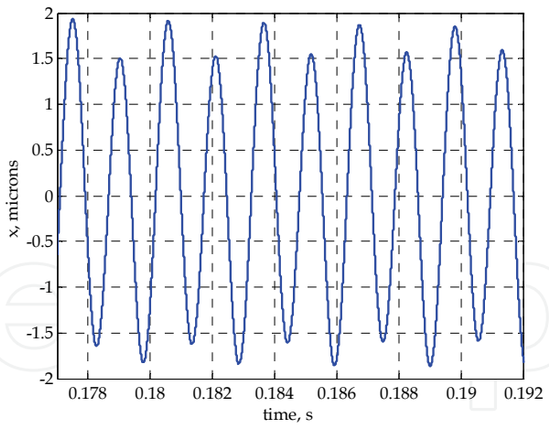

Fig. 19. The position of the shaft centre in the horizontal direction for $\varepsilon_w = 0.075$, n=39000 rpm, p_s=0.276 MPa , and 2 microns run-out

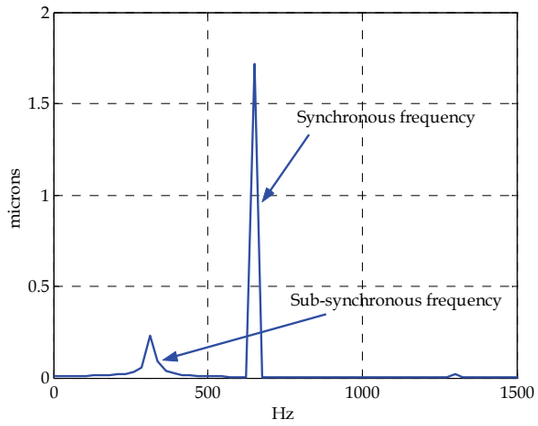

Fig. 20. FFT analysis of the motion in the horizontal direction for $\varepsilon_w = 0.075$, n=39000 rpm, p_s=0.276 MPa , and 2 microns run-out

The experiments show that the sub-synchronous frequency becomes dominant for rotational speeds greater than 44000 rpm (Fig. 21). However, the synchronous frequency is still present. The numerically predicted journal centre trajectories for a rotational speed of 44000 rpm without and with run-out are presented in Figs. (22) and (23). In both cases, the journal centre moves on closed orbits. Again, the simulation corresponding to the motion without run-out predicts only the sub-synchronous frequency (Fig. 24). The synchronous frequency is predicted only by the simulation that takes into account the small run-out (Fig. 25). In this case, the wave shape of the motion in the horizontal direction (Fig. 26) is also very similar to that predicted by experiments (Fig. 21). An increase of the oil supply pressure to 0.414 MPa stabilizes the fluid film of the bearing (Fig. 27). The theoretical analysis shows that the bearing can run stable up to 60000 rpm. The critical mass becomes greater than the rotor mass (Fig. 28). The FFT analyze of the numerical simulated motion for a rotational speed of 60000 rpm and a run-out of 2 microns is presented in Fig. (29). It can be seen that the sub-synchronous frequency disappeared. The corresponding trajectory and the motion in the horizontal direction are also presented in Figs. (30) and (31). If the run-out is zero, then the

limit cycles disappear and the journal approaches to the bearing centre and orbits around it with a very small radius (Fig. 32).
It can be noticed from all the above simulations that the wave bearing journal centre maintains its trajectory inside the bearing clearance, even for unstable motions.

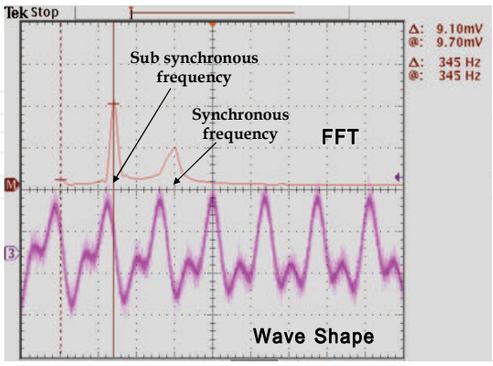

Fig. 21. FFT analysis and wave shape of the experimental signal for $\varepsilon_w = 0.075$, n=44000 rpm, p_s=0.276 MPa

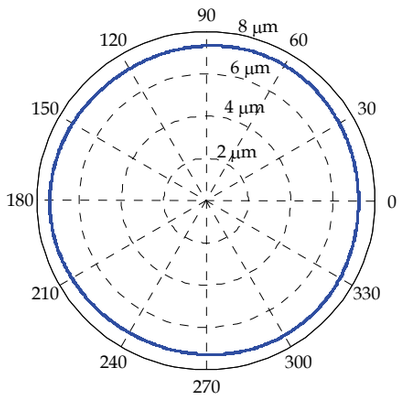

Fig. 22. Trajectory of the journal centre for $\varepsilon_w = 0.075$, n=44000 rpm, p_s=0.276 MPa , and zero run-out

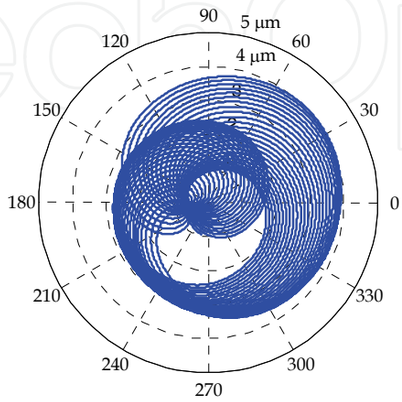

Fig. 23. Trajectory of the journal centre for $\varepsilon_w = 0.075$, n=44000 rpm, p_s=0.276 MPa , and 2 microns run-out

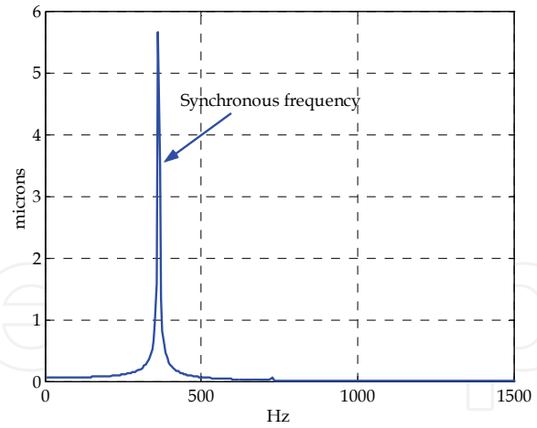

Fig. 24. FFT analysis of the motion in the horizontal direction for $\varepsilon_w = 0.075$, n=44000 rpm, ps=0.276 MPa , and zero run-out

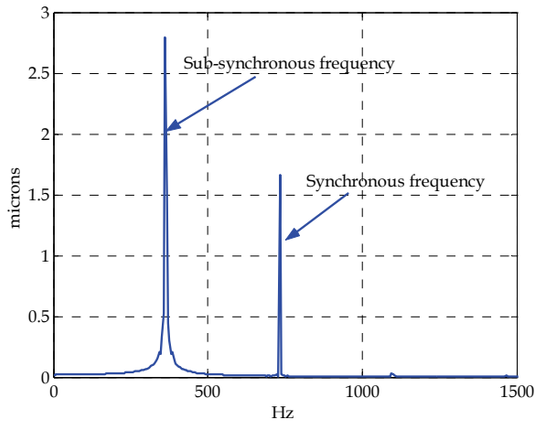

Fig. 25. FFT analysis of the motion in the horizontal direction for $\varepsilon_w = 0.075$, n=44000 rpm, p_s=0.276 MPa , and 2 microns run-out

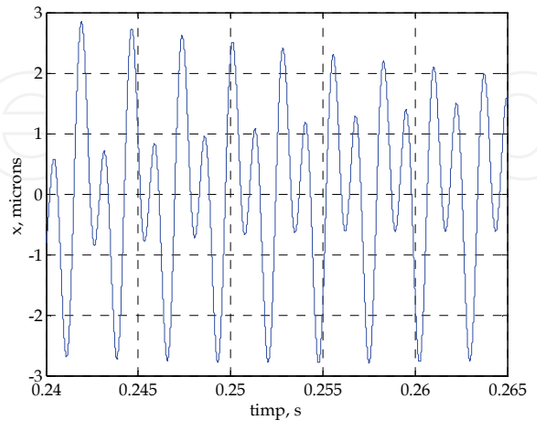

Fig. 26. The position of the shaft centre in the horizontal direction for $\varepsilon_w = 0.075$, n=44000 rpm, p_s=0.276 MPa , and 2 microns run-out

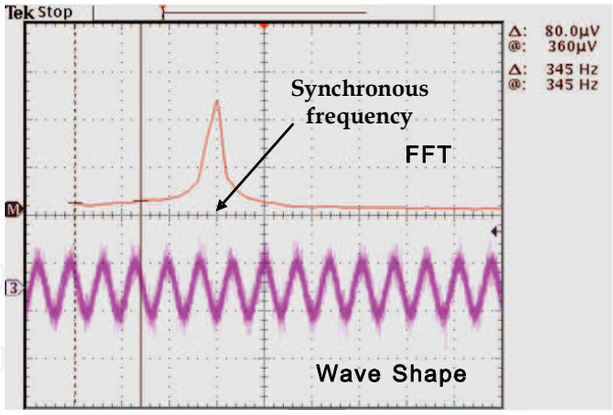

Fig. 27. FFT analysis and wave shape of the experimental signal for $\varepsilon_w = 0.075$, n=44000 rpm, p_s=0.414 MPa

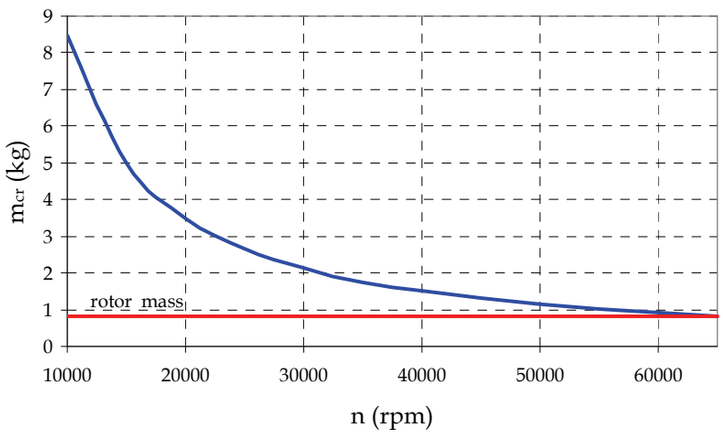

Fig. 28. Critical mass as function of running speed for $\varepsilon_w = 0.075$ and p_s=0.414 MPa

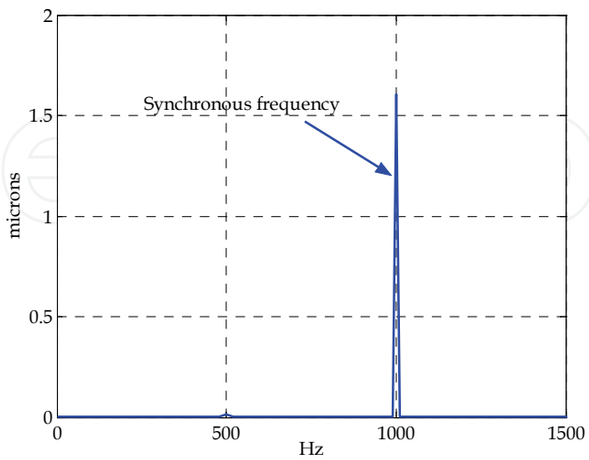

Fig. 29. FFT analysis and wave shape of the experimental signal for $\varepsilon_w = 0.075$, n=60000 rpm, p_s=0.414 MPa

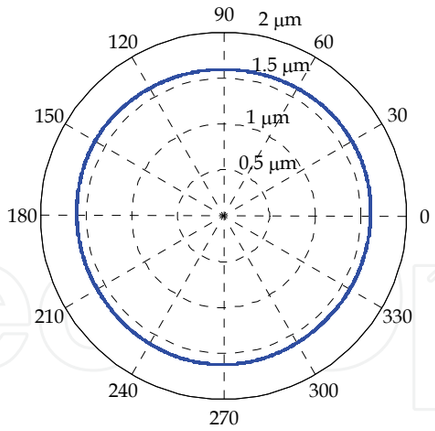

Fig. 30. Trajectory of the journal centre for $\varepsilon_w = 0.075$, n=60000 rpm, p_s=0.440 MPa, and 2 microns run-out

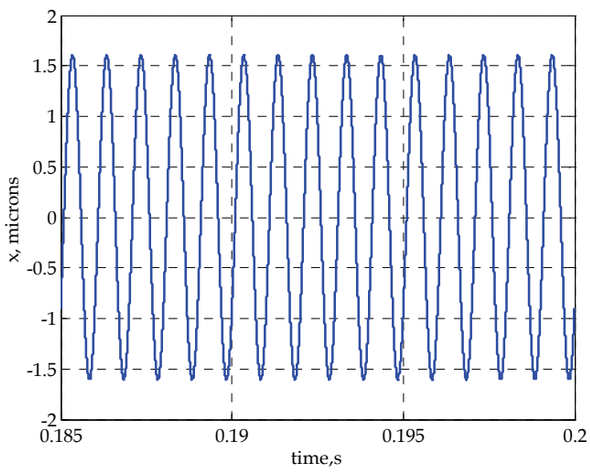

Fig. 31. The position of the shaft centre in the horizontal direction for $\varepsilon_w = 0.075$, n=60000 rpm, p_s=0.414 MPa , and 2 microns run-out

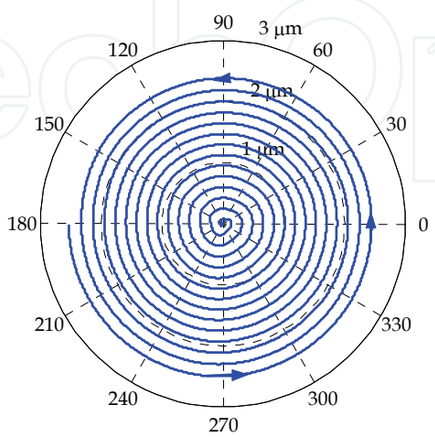

Fig. 32. Trajectory of the journal centre for $\varepsilon_w = 0.075$, n=60000 rpm, p_s=0.440 MPa, and 0 microns run-out

7. Conclusions

Both a critical mass and a transient method were developed to model and simulate the dynamic behavior of a fluid film wave journal bearing. The methods were validated by comparing the theoretical results obtained for a three-wave bearing having a diameter of 30 mm, a length of 27.5 mm and a clearance of 35 microns with experimental data. It was concluded that:

- The dynamic behavior of the bearing after the appearance of the sub-synchronous frequency could be numerically predicted only by using a transient approach.
- The experimental studies demonstrated that even when the bearing fluid film is unstable, the synchronous frequency is still present.
- The numerical simulations showed that the presence of the synchronous frequency in the unstable motions can be theoretically predicted only if the inherent unbalance of the rotor is taken into consideration.
- The theoretical and experimental investigations also proved that even if the fluid film is unstable, the wave bearing maintains the whirl orbit inside the bearing clearance.

8. References

Constantinescu, V. N., Nica, A., Pascovici, M. D., Ceptureanu, G. & Nedelcu S., (1985) *Sliding Bearings*, Allerton Press, ISBN 0-89864-011-3, New York

Dimofte, F. (1995). Wave journal bearing with compressible lubricant – Part I : The wave bearing concept and a comparison to the plain circular bearing, *Tribology Transactions*, Vol. 38, No. 1, pp. 153-160

Dimofte, F. (1995). Wave journal bearing with compressible lubricant – Part II : A comparison of the wave bearing with a groove bearing and a lobe bearing, *Tribology Transactions*, Vol. 38, No. 2, pp. 364-372

Dimofte, F. (1995). Wave journal bearing Part 1 : Analysis, NASA Report NASA-CR-19543-PT-1

Dimofte, F., Proctor, M.P., Fleming, D.P. & Keith, T. G. (2004). Experimental investigations on the influence of oil inlet pressure on the stability of wave journal bearing, *Proceedings of the 10th International Symposium on Transportation Phenomena and Dynamics of Rotating Machinery*, Honolulu, Hawaii, ISROMAC 10-2004-146

Ene, N. M., Dimofte, D. & Keith Jr., T. G. (2008). A dynamic analysis of hydrodynamic wave journal bearings, *Tribology Transactions*, Vol. 51, pp. 82-91

Frêne, J. & Constantinescu, V. N. (1975). Operating characteristics of journal bearings in the transition region, *Proceedings of the 2nd Leeds – Lyon Symposium on Tribology*, pp. 121-124

Frêne, J., Nicolas, D., Degueurce, B., Berthe, D. & Godet, M. (1997). Hydrodynamic lubrication : Bearings and thrust bearings, Elsevier, ISBN 0 444 82366 2, Amsterdam

Hashimoto, H. & Wada, S. (1990) Dynamic behavior of unbalanced rigid shaft supported on turbulent journal bearings – Theory and experiment, *ASME Journal of Tribology*, Vol. 112, pp. 404-408

Kakoty, S. K. & Majumdar, B. C., (1999). Effects of fluid inertia on stability of flexibly supported oil journal bearings: Linear perturbation analysis, *Tribology International*, Vol. 32, pp. 217-228

Kakoty, S. K. & Majumdar, B. C., (2000), Effects of fluid inertia on the dynamic coefficients and stability of journal bearings, *Proceedings IMechE, Part J*, Vol. 214, pp. 229 - 242

Kilt, P. & Lund J.W., (1986). Calculation of the dynamic coefficients of a journal bearing using a variational approach, *Journal of Tribology*, Vol. 108, pp. 421-425

Kirk, R. G. & Gunter, E. J. (1976). Short bearing analysis applied to rotordynamics I: Theory, *ASME Journal of Lubrication Technology*, Vol. 98, pp. 47-56

Kirk, R. G. & Gunter, E. J. (1976), Short bearing analysis applied to rotordynamics II: Results of journal bearing response, *ASME Journal of Lubrication Technology*, Vol. 98, pp. 319-329

Kostrzewsky G.J., Taylor D., Flack R.D. & Barrett L., (1998). Theoretical and experimental dynamic characteristics of highly preloaded three-lobe journal bearings, *Tribology Transactions*, Vol. 41, pp. 392-398

Lund, J. W. & Thomsen, K. K. (1978). A calculation method and data for the dynamic coefficients of oil–lubricated journal bearings, *Topics in Fluid Bearing and Rotor Bearing System Design and Optimization*, ASME, New York, pp. 1-28

Lund, J. W. (1987). Review of the concept of dynamic coefficients for fluid film journal bearings, *ASME Journal of Tribology*, Vol. 109, No. 37, pp. 37-41

Monmousseau, P. & Fillon, M. (1999). Frequency effects on the TEHD behavior of a tilting-pad journal bearing under dynamic loading, *ASME Journal of Tribology*, Vol. 121, pp. 321-326

Newkirk, B.L. & Taylor, H. D. (1925). Shaft whipping due to oil action in journal bearings, *General Electric Review*, Vol. 28, No. 8, pp. 985-988

Orcutt F.K. & Arwas E.B., (1967). The steady-state and dynamic characteristics of a full circular bearing and a partial arc bearing in the laminar and turbulent flow regimes, *Journal of Lubrication Technology*, pp. 143-153

Parkins D.W., (1979). Theoretical and experimental determination of the dynamic characteristics of a hydrodynamic journal bearing, *ASME Journal of Lubrication Technology*, Vol. 101, pp. 129-139

Rao T.V.V.L.N. & Sawicki J.T., (2002). Linear stability analysis for a hydrodynamic journal bearing considering cavitation effects, *STLE Tribology Transactions*, Vol. 45, No. 4, pp. 450-456

Rao T.V.V.L.N. & Sawicki J.T., (2004). Stability characteristics of herringbone grooved journal bearings incorporating cavitation effects, *ASME Journal of Tribology*, Vol. 126, pp. 281-287

San Andres, L. (1997). Transient response of externally pressurized fluid film bearings, *STLE Tribology Transactions.*, Vol. 40, No. 1, pp. 147-155

Tichy, J. & Bou-Said. B. (1991). Hydrodynamic lubrication and bearing behavior with impulsive loads, *STLE Tribology Transactions*, Vol. 34, No. 4, pp. 505-512

Tieu, A. K. & Qiu, Z. L. (1995). Stability of finite journal bearings from linear and nonlinear bearing forces, *STLE Tribology Transactions*, Vol. 38, No. 3, pp. 627-635

Vijayaraghavan, D. & Brewe & D. E., (1992). Frequency Effects on the Stability of a Journal Bearing for Periodic Loading, *ASME Journal of Tribology*, Vol. 114, pp. 107-115

White, M. F. & Chan, S. H., (1992). The sub-synchronous dynamic behavior of tilting-pad journal bearings, *Journal of Tribology*, Vol. 114, pp. 167-173

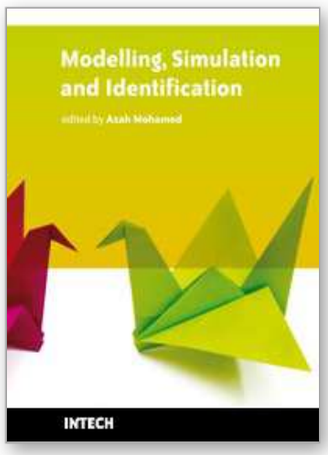

Modelling, Simulation and Identification

Edited by Azah Mohamed

ISBN 978-953-307-136-7
Hard cover, 354 pages
Publisher Sciyo
Published online 18, August, 2010
Published in print edition August, 2010

Modeling, simulation and identification has been actively researched in solving practical engineering problems. This book presents the wide applications of modeling, simulation and identification in the fields of electrical engineering, mechanical engineering, civil engineering, computer science and information technology. The book consists of 17 chapters arranged in an order reflecting multidimensionality of applications related to power system, wireless communication, image and video processing, control systems, robotics, soil mechanics, road engineering, mechanical structures and workforce capacity planning. New techniques in signal processing, adaptive control, non-linear system identification, multi-agent simulation, eigenvalue analysis, risk assessment, modeling of dynamic systems, finite difference time domain modeling and visual feedback are also presented. We hope that readers will find the book useful and inspiring by examining the recent developments in the applications of modeling, simulation and identification.

How to reference

In order to correctly reference this scholarly work, feel free to copy and paste the following:

Nicoleta Ene, Florin Dimofte and Abdollah Afjeh (2010). Modelling and Simulation of the Dynamic Behavior of an Oil Wave Journal Bearing, Modelling, Simulation and Identification, Azah Mohamed (Ed.), ISBN: 978-953-307-136-7, InTech, Available from: http://www.intechopen.com/books/modelling--simulation-and-identification/modelling-and-simulation-of-the-dynamic-behavior-of-an-oil-wave-journal-bearing

INTECH
open science | open minds

InTech Europe
University Campus STeP Ri
Slavka Krautzeka 83/A
51000 Rijeka, Croatia
Phone: +385 (51) 770 447
Fax: +385 (51) 686 166
www.intechopen.com

InTech China
Unit 405, Office Block, Hotel Equatorial Shanghai
No.65, Yan An Road (West), Shanghai, 200040, China
中国上海市延安西路65号上海国际贵都大饭店办公楼405单元
Phone: +86-21-62489820
Fax: +86-21-62489821

IntechOpen